Resolution of prestack depth migration

Luděk Klimeš

Department of Geophysics, Faculty of Mathematics and Physics, Charles University, Ke Karlovu 3, 121 16 Praha 2, Czech Republic (http://sw3d.cz/staff/klimes.htm)

Received: February 19, 2011; Revised: October 26, 2011; Accepted: January 7, 2012

ABSTRACT

The resolution of a general 3–D common–shot elastic prestack depth migration in a heterogeneous anisotropic medium is studied approximately, using the ray theory. It is demonstrated that the migrated section can approximately be represented by the convolution of the reflectivity function with the corresponding local resolution function. Alternatively, it can also be approximately represented by the convolution of the spatial distribution of the weak–contrast displacement reflection–transmission coefficient with the corresponding local resolution function. The derived explicit approximate equations enable us to predict the migration resolution approximately without doing the whole and expensive migration. The equations are applicable to 3–D elastic migrations in 3–D isotropic or anisotropic, heterogeneous velocity models.

Both the reflectivity function and the spatial distribution of the weak–contrast displacement reflection–transmission coefficient approximately determine the linear combination of the perturbations of elastic moduli and density to which the migrated section is sensitive. The imaged linear combination of the perturbations of elastic parameters depends on the selection of the polarizations (wave types) of the incident and back–propagated wavefields and on the directions of propagation.

The resolution of the linear combination of the perturbations of elastic moduli and density in the migrated section is determined by the above mentioned local resolution functions. The local resolution functions depend on the aperture and on the imaging function. The imaging function is determined by the source time function and by the form of the imaging functional. The local resolution functions are considerably sensitive to heterogeneities. The local resolution functions in elastic media differ from their acoustic counterparts, especially by the existence of converted scattered waves in elastic media.

Keywords: elastic waves, velocity model, seismic migration, resolution, wavefield inversion, seismic anisotropy, heterogeneous media

1. INTRODUCTION

A general formulation of *prestack depth migration* based on imaging (mapping) incident and scattered wavefields, extrapolated into the velocity model by arbitrary numerical methods (*Claerbout, 1971*) is considered in this paper. Therefore, a very general imaging functional is considered. This means that the paper is not devoted to a particular migration algorithm. The migration algorithm may be based, e.g., on full–wavefield methods like finite differences or on various approximate methods. We study the resolution of a general prestack depth migration approximately, using the ray theory.

A *common–shot* prestack depth migration is assumed since it is the most natural configuration from the physics point of view, although the same approach could simply be applied to other configurations. The presented theory is developed for *3–D elastic migrations* in 3–D isotropic or anisotropic, heterogeneous velocity models. Neither scalar acoustic wavefields nor 2-D migrations are investigated separately.

The purpose of this paper is to study the physical meaning and spatial resolution of the migrated images. Our resolution study is considerably more general than the resolution analyses performed by *Wu and Toksöz (1987)*, *Lecomte and Gelius (1998)* and *Lecomte (1999)* for the scalar wave equation in acoustic media with constant density.

Some of the building blocks of the resolution analysis have already been proposed by various authors. For example, the angle–dependent reflectivity function (half the scattering coefficient) has already been used in anisotropic elastic media by *Ursin and Tygel (1997, Eq. 22)* and *Ursin (2004, Eq. 12)*. For the special case of the scalar wave equation in acoustic media with constant density, the local resolution function corresponding to the angle–dependent reflectivity function (point–spread function) has been proposed by *Devaney (1984)* and *Gelius et al. (1991)*, and analytically estimated in special cases by *Gelius (1995a; 1995b)*. Hereinafter, we shall perform approximately the resolution analysis for general 3–D elastic common–shot prestack depth migrations in 3–D heterogeneous anisotropic elastic media. For this general case, we estimate the local resolution function corresponding to the angle–dependent reflectivity function, define the reflectivity function which is angle–independent, and introduce the spatial distribution of the weak–contrast displacement reflection–transmission coefficient together with the corresponding local resolution function.

Although the migrations are mostly performed in isotropic velocity models, we shall present the equations in a general form suitable for elastic waves in heterogeneous anisotropic velocity models, because the assumption of isotropic velocity models or of isotropic perturbations provide no considerable simplification of the theory (*Beylkin and Burridge, 1990*). The equations expressed in terms of the general stiffness tensor c_{ijkl} are usually more concise and clear than the analogous explicit isotropic equations.

We start with the specification of the problem. In Section 2, we define the velocity model, the structural perturbations to be imaged, and the corresponding elastodynamic equation. In Section 3, we specify the properties of a general migration algorithm to which our resolution analysis can be applied, and define a general imaging functional. In Section 4, we introduce and apply the Born approximation and the high–frequency ray–theory approximations, which we are using to estimate approximately the resolution of the common–shot prestack depth migrated section. In Section 5, we insert the approximations of Section 4 into the imaging functional and derive the final equations which are highlighted by frames. In Section 5.1, we define the imaging function corresponding to the general imaging functional and to the incident waveform. This imaging function determines the form of the resolution functions. In Section 5.2, we insert the approximations of Section 4 into the imaging functional. Sections 5.3 and 5.4 are devoted to the final results of the resolution analysis. In Section 5.3, we define the reflectivity function which is angle–independent, and the corresponding local resolution function. In Section 5.4, we define the spatial distribution of the weak–contrast displacement reflection–transmission coefficient, and the corresponding local resolution function. Refer to the Conclusions for the discussion of the results.

We use both vectorial and componental notation. For example, either $\mathbf{x}$ or x_i may stand for three spatial coordinates x_1, x_2, x_3. The Einstein summation over repetitive lower–case Roman subscripts corresponding to the 3 spatial coordinates is used throughout the paper.

2. VELOCITY MODEL AND THE ELASTODYNAMIC EQUATION

The velocity model of the geological structure is described in terms of the material parameters

$$\varrho = \varrho(\mathbf{x}) \ , \quad c_{ijkl} = c_{ijkl}(\mathbf{x}) \ , \tag{1}$$

where $\mathbf{x} = (x_1, x_2, x_3)$ are spatial coordinates, ϱ is the density and c_{ijkl} are the elastic moduli. We assume that velocity model $\varrho(\mathbf{x})$ and $c_{ijkl}(\mathbf{x})$ is smooth.

The actual geological structure is described in terms of the unknown material parameters

$$\varrho(\mathbf{x}) + \delta\varrho(\mathbf{x}) \ , \quad c_{ijkl}(\mathbf{x}) + \delta c_{ijkl}(\mathbf{x}) \ , \tag{2}$$

where $\delta\varrho(\mathbf{x})$ and $\delta c_{ijkl}(\mathbf{x})$ represent the differences between the geological structure and the velocity model. Differences $\delta\varrho(\mathbf{x})$ and $\delta c_{ijkl}(\mathbf{x})$ are assumed to be small, but their dependence on coordinates $\mathbf{x}$ may be rough.

Seismic wavefield $u_i(\mathbf{x}, t)$ in the velocity model is subject to the elastodynamic equation

$$\varrho(\mathbf{x}) \ \ddot{u}_i(\mathbf{x}, t) = [c_{ijkl}(\mathbf{x}) \ u_{k,l}(\mathbf{x}, t)]_{,j} + f_i(\mathbf{x}, t) \tag{3}$$

for displacement $u_i(\mathbf{x}, t)$, where the dot $\dot{}$ stands for the derivative with respect to time t, and subscript $_{,j}$ following a comma stands for the partial derivative with

respect to Cartesian spatial coordinate x_j. Term $f_i(\mathbf{x},t)$ represents the source of the wavefield.

First–order perturbation (variation) δ of elastodynamic equation (3) yields the elastodynamic equation

$$\varrho(\mathbf{x})\ \delta\ddot{u}_i(\mathbf{x},t) = [c_{ijkl}(\mathbf{x})\ \delta u_{k,l}(\mathbf{x},t)]_{,j} - \delta\varrho(\mathbf{x})\ \ddot{u}_i(\mathbf{x},t) + [\delta c_{ijkl}(\mathbf{x})\ u_{k,l}(\mathbf{x},t)]_{,j} \quad (4)$$

for the first–order wavefield perturbation $\delta u_i(\mathbf{x},t)$ due to medium perturbations $\delta c_{ijkl}(\mathbf{x})$ and $\delta\varrho(\mathbf{x})$. We shall refer to $\delta u_i(\mathbf{x},t)$ as the *scattered wavefield*.

Elastodynamic Green tensor $G_{km}(\mathbf{x},\mathbf{x}',t)$, corresponding to elastodynamic equation (1) in the velocity model, is defined by equation (*Červený, 2001, Eq. 2.5.37*)

$$\varrho(\mathbf{x})\ \ddot{G}_{im}(\mathbf{x},\mathbf{x}',t-t') = [c_{ijkl}(\mathbf{x})\ G_{km,l}(\mathbf{x},\mathbf{x}',t-t')]_{,j} + \delta_{im}\,\delta(\mathbf{x}-\mathbf{x}')\,\delta(t-t') \quad (5)$$

with the zero initial conditions for $t-t' \leq 0$. The spatial partial derivatives in elastodynamic equation (5) are related to coordinates x_i. Here $\delta(\mathbf{x})$ and $\delta(t)$ are the 3–D and 1–D Dirac distributions.

In this paper, we shall mostly work in the frequency domain with 1–D Fourier transform

$$\widehat{u}_i(\mathbf{x},\omega) = \widehat{\delta}(\omega)\int \mathrm{d}t\ u_i(\mathbf{x},t)\ \exp(\mathrm{i}\omega t) \quad (6)$$

of the displacement, and with the analogous Fourier transform of the elastodynamic Green tensor. Here $\widehat{\delta}(\omega)$ is a constant equal to the 1–D Fourier transform of the 1–D Dirac distribution $\delta(t)$.

3. MIGRATION

In our approach, prestack depth migration may be decomposed into the following steps (*Claerbout, 1971*): (a) *extrapolation* of the wavefields from the source and receiver points into the velocity model, (b) *decomposition* of the extrapolated wavefields into waves of different types or even of different properties, (c) *imaging* the extrapolated and decomposed wavefields.

3.1. Extrapolation

Assume that seismic wavefield $u_i(\mathbf{x}'',t)+\delta u_i(\mathbf{x}'',t)$ is recorded at the receivers covering the *receiver area* along the Earth surface with a sufficient receiver density to allow for the back propagation of scattered wavefield $\delta u_i(\mathbf{x}'',t)$ into the velocity model. Scattered wavefield $\delta u_i(\mathbf{x}'',t)$ is approximated by the solution of elastodynamic equation (4) for the first–order wavefield perturbation.

Let us denote by $U_i(\mathbf{x},t)$ the scattered wavefield $\delta u_i(\mathbf{x}'',t)$ back–propagated from the receiver area into the velocity model. Note that we do not back–propagate the complete scattered wavefield but only its part recorded in the receiver area. Moreover, the recorded wavefield may also be reduced by application of the aperture weighting factor $a(\mathbf{x}'')$ dependent on the receiver positions $\mathbf{x}''$.

Note that both incident wavefield $u_i(\mathbf{x}'', t)$ and back–propagated scattered wavefield $U_i(\mathbf{x}, t)$ may be calculated by arbitrary numerical methods, including, e.g., finite differences, although our approximate resolution analysis is based on the ray theory.

In the time domain, we can back–propagate the scattered wavefield by taking the scattered wavefield at the receivers with opposite time, propagating it into the target zone using the representation theorem, and then changing the sign of time again. The opposite time in the time domain corresponds to the complex–conjugate wavefield in the frequency domain. In the frequency domain, we thus take the complex–conjugate scattered wavefield at the receivers, insert it together with the Green tensor into the representation theorem, and complex–conjugate the result.

In the frequency domain, the forward propagation from point $\mathbf{x}'$ (actual scatterer) situated in the vicinity of point $\mathbf{x}$ (position in the migrated section) to point $\mathbf{x}''$ situated on the surface covered by the receivers is described by Green tensor $\widehat{G}_{im}(\mathbf{x}'', \mathbf{x}', \omega)$. The back propagation from point $\mathbf{x}''$ to point $\mathbf{x}$ is then described by complex–conjugate Green tensor $\widehat{G}^*_{in}(\mathbf{x}, \mathbf{x}'', \omega) = \widehat{G}^*_{ni}(\mathbf{x}'', \mathbf{x}, \omega)$.

The scattered wavefield can be back–propagated from surface S to point $\mathbf{x}$ using the frequency–domain representation theorem (*Červený, 2001, Eq. 2.6.4*):

$$\widehat{U}_i(\mathbf{x}, \omega) = \frac{1}{\widehat{\delta}(\omega)} \int_S \mathrm{d}S(\mathbf{x}'')\, a(\mathbf{x}'') \left[\widehat{G}^*_{ni}(\mathbf{x}'', \mathbf{x}, \omega)\, n_j(\mathbf{x}'')\, c_{njkl}(\mathbf{x}'')\, \widehat{\delta u}_{k,l}(\mathbf{x}'', \omega) - \widehat{G}^*_{ni,j}(\mathbf{x}'', \mathbf{x}, \omega)\, c_{njkl}(\mathbf{x}'')\, \widehat{\delta u}_k(\mathbf{x}'', \omega)\, n_l(\mathbf{x}'') \right] , \tag{7}$$

where $\widehat{\delta}(\omega)$ is a constant equal to the 1–D Fourier transform of the 1–D Dirac distribution $\delta(t)$. Note that *Červený (2001)* chose $\widehat{\delta}(\omega) = 1$. Unit normal $n_j(\mathbf{x}'')$ to surface S is pointing in accord with the forward propagation of the incident wavefield. The partial derivatives in Eq. (7) are related to variable $\mathbf{x}''$. The weighting factor of $a(\mathbf{x}'')$ is inserted to account for possible windowing of the seismic records (time sections) at receiver points $\mathbf{x}''$. If we do not need windowing of the seismic records, we may put $a(\mathbf{x}'') = 1$. Note that the target zone is situated inside formally closed surface S, and that the volume integral from the representation theorem is not present in Eq. (7) because of back propagation from the receiver area only.

The approximate incident wavefield $u_i(\mathbf{x}, t)$ and the back–propagated scattered wavefield $U_i(\mathbf{x}, t)$ may be calculated in velocity model $\varrho(\mathbf{x})$, $c_{ijkl}(\mathbf{x})$ by any convenient numerical method.

3.2. Decomposition

To resolve more than a single linear combination of medium perturbations $\delta\varrho(\mathbf{x})$ and $\delta c_{ijkl}(\mathbf{x})$, it is desirable to attempt to decompose both the approximate incident wavefield $u_i(\mathbf{x}, t)$ and the back–propagated scattered wavefield $U_i(\mathbf{x}, t)$ at each point $\mathbf{x}$ locally into P and S waves or, better, into P waves and two polarizations of S waves. Such a decomposition may conveniently be accomplished by a proper choice of imaging functionals.

In addition, if the waves incident from considerably different directions can locally be distinguished in the approximate incident wavefield $u_i(\mathbf{x},t)$ or back–propagated scattered wavefield $U_i(\mathbf{x},t)$, the respective wavefield may be decomposed into the parts corresponding to the different propagation directions, particularly for the purposes of the "amplitude–versus–angle" analysis.

If the decomposition is not made correctly, we obtain ghosts in the migrated section. For example, if a part of an S wave is back–propagated as a P wave, the correct migrated section is combined with a false migrated section.

The decomposition might be unnecessary for a full–wavefield (e.g., finite–difference) migration if we had an exact velocity model. Unfortunately, since the velocity model is only approximate, we may need the decomposition even for a full–wavefield migration.

If the decomposition into the parts corresponding to the different propagation directions is not possible, the amplitude–versus–angle analysis may be facilitated by splitting the receiver area into two or more smaller receiver areas, e.g., by applying the aperture weighting factor $a(\mathbf{x}'')$ dependent on receiver positions $\mathbf{x}''$. This splitting, however, deteriorates the lateral spatial resolution of the migrated sections.

If any of the above decompositions is applicable, let $u_i(\mathbf{x},t)$ denote hereinafter one selected part of the decomposed approximate incident wavefield and $U_i(\mathbf{x},t)$ one selected part of the back–propagated scattered wavefield.

3.3. Imaging

We have, at each point $\mathbf{x}$, time functions $u_i(\mathbf{x},t)$ and $U_i(\mathbf{x},t)$ representing selected parts of the incident wavefield and of the back–propagated scattered wavefield.

Assume that *imaging functional* (mapping procedure)

$$M(\bullet,\bullet): \quad u_i, U_j \longrightarrow m = M(u_i, U_j) \tag{8}$$

maps the pairs of functions $u_i = u_i(t')$ and $U_j = U_j(t)$ onto the real or complex numbers. In definition (8), the first argument $u_i = u_i(\mathbf{x},t')$ represents the incident wavefield and the second argument $U_j = U_j(\mathbf{x},t)$ represents the back–propagated scattered wavefield. These wavefields may be calculated by any suitable numerical method.

The *migrated section* is then (*Claerbout, 1971*)

$$m(\mathbf{x}) = M\big(u_i(\mathbf{x},t'), U_j(\mathbf{x},t)\big) \quad . \tag{9}$$

We assume that the imaging functional (8) is linear with respect to the second argument representing the back–propagated scattered wavefield.

4. BORN APPROXIMATION OF THE BACK–PROPAGATED SCATTERED WAVEFIELD

4.1. Born Approximation of the Scattered Wavefield

The wavefield scattered by medium perturbations $\delta c_{ijkl}(\mathbf{x})$ and $\delta\varrho(\mathbf{x})$ can be approximated by the solution $\delta u(\mathbf{x}'', t)$ of elastodynamic equation (4). The Fourier transform $\widehat{\delta u}_i(\mathbf{x}'', \omega)$ of scattered wavefield $\delta u(\mathbf{x}'', t)$ can be expressed in the form of the first–order Born approximation (*Červený, 2001, Eq. 2.6.18*)

$$\widehat{\delta u}_i(\mathbf{x}'', \omega) \approx \frac{1}{\widehat{\delta}(\omega)} \int \mathrm{d}\mathbf{x}' \Big[- \widehat{G}_{im,j}(\mathbf{x}'', \mathbf{x}', \omega)\, \delta c_{mjkl}(\mathbf{x}')\, \widehat{u}_{k,l}(\mathbf{x}', \omega) - (\mathrm{i}\omega)^2\, \widehat{G}_{im}(\mathbf{x}'', \mathbf{x}', \omega)\, \delta\varrho(\mathbf{x}')\, \widehat{u}_m(\mathbf{x}', \omega) \Big] \quad , \tag{10}$$

where the partial derivatives are related to variable $\mathbf{x}'$. Here $\widehat{\delta}(\omega)$ is a constant equal to the 1–D Fourier transform of the 1–D Dirac distribution $\delta(t)$. Note that *Červený (2001)* chose $\widehat{\delta}(\omega) = 1$. The integration in Eq. (10) is performed over the whole volume in which $\delta c_{mjkl}(\mathbf{x}')$ and $\delta\varrho(\mathbf{x}')$ are non–vanishing.

4.2. Decomposing the Incident Wave into Arrivals and the Green Tensor into Elementary Waves

We assume that incident wavefield $\widehat{u}_i(\mathbf{x}', \omega)$ in Eq. (10) is composed of several arrivals $\widehat{u}_m^{\mathrm{Arr}}(\mathbf{x}', \omega)$,

$$\widehat{u}_i(\mathbf{x}', \omega) = \sum_{\mathrm{Arr}} \widehat{u}_i^{\mathrm{Arr}}(\mathbf{x}', \omega) \quad . \tag{11}$$

Then also the scattered wavefield is composed of several arrivals.

The ray–theory approximation of the wavefield is composed of contributions called elementary waves. These elementary waves may represent various seismic body waves, such as direct, reflected, converted or multiply reflected/transmitted waves. The ray–theory approximation of the Green tensor is thus composed of the elementary Green tensors corresponding to the individual elementary waves:

$$\widehat{G}_{im}(\mathbf{x}'', \mathbf{x}, \omega) = \sum_{\mathrm{EW}} \widehat{G}_{im}^{\mathrm{EW}}(\mathbf{x}'', \mathbf{x}, \omega) \quad . \tag{12}$$

The corresponding prestack depth migrated section is then composed of the migrated sections corresponding to all combinations of the above mentioned arrivals and elementary waves:

$$\widehat{m}(\mathbf{x}) = \sum_{\mathrm{Arr}} \sum_{\mathrm{EW}} \widehat{m}^{\mathrm{ArrEW}}(\mathbf{x}) \quad . \tag{13}$$

In the following, we shall consider just one of the arrivals and one of the elementary waves, but omit superscripts $^{\mathrm{Arr}}$ and $^{\mathrm{EW}}$ for the sake of conciseness and simplicity.

In the following, we shall also assume that each arrival of the incident wave can be expressed in terms of unit polarization vector $E_k(\mathbf{x}')$ and local spectrum $\widehat{f}(\mathbf{x}',\omega)$:

$$\widehat{u}_k^{\mathrm{Arr}}(\mathbf{x}',\omega) = E_k(\mathbf{x}')\,\widehat{f}(\mathbf{x}',\omega) \quad . \tag{14}$$

4.3. Ray–Theory Approximation of the Green Tensor

We shall now apply the ray–theory approximation of the Green tensor. We parametrize the rays from point $\mathbf{x}$ to point $\mathbf{x}''$ by the initial slowness vectors at point $\mathbf{x}$. The rays corresponding to the small area $\mathrm{d}S_p(\mathbf{x})$ situated on the slowness surface then create a narrow ray tube. We denote by $\mathrm{d}S_\perp(\mathbf{x}'')$ the area of the perpendicular cross–section of this ray tube at point $\mathbf{x}''$. The relative geometrical spreading of *Červený (2001, Eq. 4.14.45)* then reads

$$L(\mathbf{x}'',\mathbf{x}) = \sqrt{\frac{v(\mathbf{x}'')v(\mathbf{x})\,\mathrm{d}S_\perp(\mathbf{x}'')}{c(\mathbf{x}'')c(\mathbf{x})\,\mathrm{d}S_p(\mathbf{x})}} \tag{15}$$

(*Schleicher et al., 2001, Eq. 8*), where c is the phase velocity and v is the ray velocity (incorrectly called group velocity by some people), both corresponding to the ray leading from point $\mathbf{x}$ to point $\mathbf{x}''$.

Note that the slowness surface at point $\mathbf{x}$ may be parametrized by coordinates $\boldsymbol{\gamma} = (\gamma_1,\gamma_2)$ along the unit sphere composed of the normalized initial slowness vectors $\mathbf{p}(\mathbf{x})/|\mathbf{p}(\mathbf{x})|$. Then $\mathbf{p}(\mathbf{x}) = \mathbf{p}(\mathbf{x},\boldsymbol{\gamma})$. The small area $\mathrm{d}S_p(\mathbf{x})$ situated on the slowness surface corresponding to small area $\mathrm{d}\Gamma$ situated on the unit sphere is determined by relation

$$\frac{\mathrm{d}S_p(\mathbf{x})}{\mathrm{d}\Gamma} = \frac{v(\mathbf{x},\boldsymbol{\gamma})}{[c(\mathbf{x},\boldsymbol{\gamma})]^3} \quad . \tag{16}$$

Note that the corresponding area on the sphere of radius $|\mathbf{p}|$ is $\mathrm{d}S_\Gamma(\mathbf{x}) = \mathrm{d}\Gamma/[c(\mathbf{x},\boldsymbol{\gamma})]^2$, and the corresponding area on the slowness surface is $\mathrm{d}S_p(\mathbf{x}) = \mathrm{d}S_\Gamma(\mathbf{x})/\cos(\theta)$, where $\cos(\theta) = c(\mathbf{x},\boldsymbol{\gamma})/v(\mathbf{x},\boldsymbol{\gamma})$ is the cosine of the angle between the normals to the unit sphere and the slowness surface.

The ray–theory approximation of the elementary Green tensor corresponding to a particular elementary wave from point $\mathbf{x}$ to receiver $\mathbf{x}''$ reads (*Červený, 2001, Eq. 5.4.24*):

$$\widehat{G}_{im}(\mathbf{x}'',\mathbf{x},\omega) \approx \widehat{\delta}(\omega)\frac{e_i(\mathbf{x}'',\boldsymbol{\gamma})e_m(\mathbf{x},\boldsymbol{\gamma})T(\mathbf{x}'',\mathbf{x})}{4\pi L(\mathbf{x}'',\mathbf{x})\sqrt{\varrho(\mathbf{x}'')c(\mathbf{x}'',\boldsymbol{\gamma})\varrho(\mathbf{x})c(\mathbf{x},\boldsymbol{\gamma})}}\ \exp[\mathrm{i}\omega\tau(\mathbf{x}'',\mathbf{x})] \quad , \tag{17}$$

where e_k is the unit polarization vector and c is the phase velocity. Here $T(\mathbf{x}'',\mathbf{x})$ is the accumulated reciprocal transmission coefficient describing the amplitude losses between points $\mathbf{x}$ and $\mathbf{x}''$ due to attenuation and due to reflections and scattering into directions leading outside the vicinity of point $\mathbf{x}''$. In an ideal case, $T(\mathbf{x}'',\mathbf{x}) \approx 1$. Possible phase shifts due to caustics are also included in $T(\mathbf{x}'',\mathbf{x})$, but are annulled by the combination of forward propagation and back propagation. For $\omega < 0$,

$T(\mathbf{x}'',\mathbf{x})$ is complex–conjugate, but this complex–conjugacy is compensated by the combination of forward propagation and back propagation.

Since points $\mathbf{x}$ (position in the migrated section) and $\mathbf{x}'$ (actual scatterer) are close, quantities $\boldsymbol{\gamma}$, $e_i(\mathbf{x}'',\boldsymbol{\gamma})$, $e_m(\mathbf{x},\boldsymbol{\gamma})$, $T(\mathbf{x}'',\mathbf{x})$, $L(\mathbf{x}'',\mathbf{x})$, $c(\mathbf{x}'',\boldsymbol{\gamma})$, $c(\mathbf{x},\boldsymbol{\gamma})$ corresponding to the ray from $\mathbf{x}$ to $\mathbf{x}''$, and quantities $\boldsymbol{\gamma}'$, $e_i(\mathbf{x}'',\boldsymbol{\gamma}')$, $e_m(\mathbf{x}',\boldsymbol{\gamma}')$, $T(\mathbf{x}'',\mathbf{x}')$, $L(\mathbf{x}'',\mathbf{x}')$, $c(\mathbf{x}'',\boldsymbol{\gamma}')$, $c(\mathbf{x}',\boldsymbol{\gamma}')$ corresponding to the ray from $\mathbf{x}'$ to $\mathbf{x}''$, are approximately equal. On the other hand, the difference between two–point travel times $\tau(\mathbf{x}'',\mathbf{x})$ and $\tau(\mathbf{x}'',\mathbf{x}')$ is essential for our study.

We apply the high–frequency approximation of the spatial derivatives of the Green tensor and of the incident wavefield:

$$\frac{\partial \widehat{G}_{im}}{\partial x''_j}(\mathbf{x}'',\mathbf{x},\omega) \approx \mathrm{i}\omega p_j(\mathbf{x}'',\boldsymbol{\gamma})\, \widehat{G}_{im}(\mathbf{x}'',\mathbf{x},\omega) \quad , \tag{18}$$

$$\frac{\partial \widehat{G}_{im}}{\partial x'_j}(\mathbf{x}'',\mathbf{x}',\omega) \approx -\mathrm{i}\omega p_j(\mathbf{x}',\boldsymbol{\gamma}')\, \widehat{G}_{im}(\mathbf{x}'',\mathbf{x}',\omega) \quad , \tag{19}$$

$$\widehat{u}_{k,l}(\mathbf{x}',\omega) \approx \mathrm{i}\omega P_l(\mathbf{x}')\, \widehat{u}_k(\mathbf{x}',\omega) \quad . \tag{20}$$

Angular coordinates $\boldsymbol{\gamma}$ correspond to the ray leading from point $\mathbf{x}$ to point $\mathbf{x}''$, whereas angular coordinates $\boldsymbol{\gamma}'$ correspond to the ray leading from point $\mathbf{x}'$ to point $\mathbf{x}''$. Since points $\mathbf{x}$ and $\mathbf{x}'$ are close, $\boldsymbol{\gamma}' \approx \boldsymbol{\gamma}$. Slowness vectors $p_j(\mathbf{x}'',\boldsymbol{\gamma})$ and $p_j(\mathbf{x}',\boldsymbol{\gamma}')$ at points $\mathbf{x}''$ and $\mathbf{x}'$ correspond to the Green tensors. Slowness vector $P_l(\mathbf{x}')$ corresponds to the incident wavefield.

We insert approximations (19) and (20) into Born approximation (10):

$$\widehat{\delta u}_i(\mathbf{x}'',\omega) \approx \frac{(\mathrm{i}\omega)^2}{\widehat{\delta}(\omega)} \int \mathrm{d}\mathbf{x}'\; \widehat{G}_{im}(\mathbf{x}'',\mathbf{x}',\omega) \Big[\delta c_{mjkl}(\mathbf{x}') p_j(\mathbf{x}',\boldsymbol{\gamma}') \widehat{u}_k(\mathbf{x}',\omega) P_l(\mathbf{x}') - \delta\varrho(\mathbf{x}') \widehat{u}_m(\mathbf{x}',\omega) \Big] \quad . \tag{21}$$

4.4. Back–Propagating Scattered Wavefield

We insert approximation (21) of the scattered wavefield into back propagation (7) and obtain

$$\widehat{U}_i(\mathbf{x},\omega) \approx \frac{(\mathrm{i}\omega)^2}{\widehat{\delta}(\omega)} \int \mathrm{d}\mathbf{x}'\; \widehat{D}_{im}(\mathbf{x},\mathbf{x}',\omega) \Big[\delta c_{mjkl}(\mathbf{x}') p_j(\mathbf{x}',\boldsymbol{\gamma}') \widehat{u}_k(\mathbf{x}',\omega) P_l(\mathbf{x}') - \delta\varrho(\mathbf{x}') \widehat{u}_m(\mathbf{x}',\omega) \Big] \quad , \tag{22}$$

where

$$\widehat{D}_{im}(\mathbf{x},\mathbf{x}',\omega) = \frac{1}{\widehat{\delta}(\omega)} \int_S \mathrm{d}S(\mathbf{x}'')\, a(\mathbf{x}'') \Big[\widehat{G}^*_{ni}(\mathbf{x}'',\mathbf{x},\omega)\, n_j(\mathbf{x}'')\, c_{njkl}(\mathbf{x}'')\, \widehat{G}_{km,l}(\mathbf{x}'',\mathbf{x}',\omega) - \widehat{G}^*_{ni,j}(\mathbf{x}'',\mathbf{x},\omega)\, c_{njkl}(\mathbf{x}'')\, \widehat{G}_{km}(\mathbf{x}'',\mathbf{x}',\omega)\, n_l(\mathbf{x}'') \Big] \tag{23}$$

is the Green tensor from point $\mathbf{x}'$, back–propagated from the receiver array to point $\mathbf{x}$ situated close to point $\mathbf{x}'$. The partial derivatives in Eq. (23) are related to variable $\mathbf{x}''$.

We insert high–frequency approximation (18) into Eq. (23) and obtain

$$\widehat{D}_{im}(\mathbf{x},\mathbf{x}',\omega) \approx \frac{\mathrm{i}\omega}{\widehat{\delta}(\omega)} \int_S \mathrm{d}S(\mathbf{x}'')\, a(\mathbf{x}'')\, \widehat{G}^*_{ni}(\mathbf{x}'',\mathbf{x},\omega)\, \widehat{G}_{km}(\mathbf{x}'',\mathbf{x}',\omega) \times \left[n_j(\mathbf{x}'')\, c_{njkl}(\mathbf{x}'')\, p_l(\mathbf{x}'',\boldsymbol{\gamma}) + p_j(\mathbf{x}'',\boldsymbol{\gamma})\, c_{njkl}(\mathbf{x}'')\, n_l(\mathbf{x}'') \right] . \tag{24}$$

We insert ray–theory approximation (17) for both the Green tensors, apply approximation

$$e_k(\mathbf{x}'',\boldsymbol{\gamma}') \approx e_k(\mathbf{x}'',\boldsymbol{\gamma}) \quad , \tag{25}$$

and use identity (*Červený, 2001, Eq. 2.4.46*)

$$c_{njkl}(\mathbf{x}'') e_n(\mathbf{x}'',\boldsymbol{\gamma}) e_k(\mathbf{x}'',\boldsymbol{\gamma}) p_l(\mathbf{x}'',\boldsymbol{\gamma}) = \varrho(\mathbf{x}'')\, v_j(\mathbf{x}'',\boldsymbol{\gamma}) \quad , \tag{26}$$

where v_j is the ray–velocity vector. Equation (24) then reads

$$\widehat{D}_{im}(\mathbf{x},\mathbf{x}',\omega) \approx \mathrm{i}\omega\widehat{\delta}(\omega) \int_S \mathrm{d}S(\mathbf{x}'')\, a(\mathbf{x}'') \times \frac{2\, n_j(\mathbf{x}'')\, v_j(\mathbf{x}'',\boldsymbol{\gamma})\, e_i(\mathbf{x},\boldsymbol{\gamma}) e_m(\mathbf{x}',\boldsymbol{\gamma}') T^*(\mathbf{x}'',\mathbf{x}) T(\mathbf{x}'',\mathbf{x}')}{16\pi^2 L(\mathbf{x}'',\mathbf{x}) L(\mathbf{x}'',\mathbf{x}') \sqrt{c(\mathbf{x}'',\boldsymbol{\gamma}) \varrho(\mathbf{x}) c(\mathbf{x},\boldsymbol{\gamma}) c(\mathbf{x}'',\boldsymbol{\gamma}') \varrho(\mathbf{x}') c(\mathbf{x}',\boldsymbol{\gamma}')}} \times \exp\{\mathrm{i}\omega[\tau(\mathbf{x}'',\mathbf{x}') - \tau(\mathbf{x}'',\mathbf{x})]\} \quad . \tag{27}$$

We now apply approximations

$$\begin{aligned} T(\mathbf{x}'',\mathbf{x}') &\approx T(\mathbf{x}'',\mathbf{x}) \quad , \\ L(\mathbf{x}'',\mathbf{x}') &\approx L(\mathbf{x}'',\mathbf{x}) \quad , \\ c(\mathbf{x}'',\boldsymbol{\gamma}') &\approx c(\mathbf{x}'',\boldsymbol{\gamma}) \quad , \\ c(\mathbf{x}',\boldsymbol{\gamma}') &\approx c(\mathbf{x},\boldsymbol{\gamma}) \quad , \\ \rho(\mathbf{x}) &\approx \rho(\mathbf{x}') \end{aligned} \tag{28}$$

to the accumulated reciprocal transmission coefficient, relative geometrical spreading, phase velocities and density, and obtain

$$\widehat{D}_{im}(\mathbf{x},\mathbf{x}',\omega) \approx \frac{\mathrm{i}\omega\widehat{\delta}(\omega)}{8\pi^2} \int_S \mathrm{d}S(\mathbf{x}'')\, a(\mathbf{x}'') \frac{n_j(\mathbf{x}'')\, v_j(\mathbf{x}'',\boldsymbol{\gamma})\, e_i(\mathbf{x},\boldsymbol{\gamma}) e_m(\mathbf{x}',\boldsymbol{\gamma}') |T(\mathbf{x}'',\mathbf{x})|^2}{[L(\mathbf{x}'',\mathbf{x})]^2 c(\mathbf{x}'',\boldsymbol{\gamma}) \varrho(\mathbf{x}') c(\mathbf{x},\boldsymbol{\gamma})} \times \exp\{\mathrm{i}\omega[\tau(\mathbf{x}'',\mathbf{x}') - \tau(\mathbf{x}'',\mathbf{x})]\} \quad . \tag{29}$$

We insert Eq. (15) and relation

$$n_j(\mathbf{x}'')\, v_j(\mathbf{x}'',\boldsymbol{\gamma}) = \frac{\mathrm{d}S_\perp(\mathbf{x}'')}{\mathrm{d}S(\mathbf{x}'')}\, v(\mathbf{x}'',\boldsymbol{\gamma}) \tag{30}$$

between the area $\mathrm{d}S_\perp(\mathbf{x}'')$ of the perpendicular cross–section of a narrow ray tube and the area $\mathrm{d}S(\mathbf{x}'')$ of the cross–section of the narrow ray tube with the surface S of integration into approximation (29):

$$\widehat{D}_{im}(\mathbf{x},\mathbf{x}',\omega) \approx \frac{\mathrm{i}\omega\widehat{\delta}(\omega)}{8\pi^2} \int_S \mathrm{d}S(\mathbf{x}'')\, a(\mathbf{x}'') \frac{\mathrm{d}S_p(\mathbf{x})}{\mathrm{d}S(\mathbf{x}'')} \frac{e_i(\mathbf{x},\boldsymbol{\gamma}) e_m(\mathbf{x}',\boldsymbol{\gamma}') |T(\mathbf{x}'',\mathbf{x})|^2}{v(\mathbf{x},\boldsymbol{\gamma}) \varrho(\mathbf{x}')} \times \exp\{\mathrm{i}\omega[\tau(\mathbf{x}'',\mathbf{x}') - \tau(\mathbf{x}'',\mathbf{x})]\} \quad . \tag{31}$$

We apply Eq. (16) and the first–order paraxial approximation

$$\tau(\mathbf{x}'',\mathbf{x}') - \tau(\mathbf{x}'',\mathbf{x}) \approx -p_k(\mathbf{x},\boldsymbol{\gamma})\,(x'_k - x_k) \tag{32}$$

of the travel time at point $\mathbf{x}$, and obtain relation

$$\widehat{D}_{im}(\mathbf{x},\mathbf{x}',\omega) \approx \frac{\mathrm{i}\omega\widehat{\delta}(\omega)}{8\pi^2}\int_S \mathrm{d}S(\mathbf{x}'')\,a(\mathbf{x}'')\,\frac{\mathrm{d}\Gamma}{\mathrm{d}S(\mathbf{x}'')}\,\frac{e_i(\mathbf{x},\boldsymbol{\gamma})e_m(\mathbf{x}',\boldsymbol{\gamma}')|T(\mathbf{x}'',\mathbf{x})|^2}{[c(\mathbf{x},\boldsymbol{\gamma})]^3\,\varrho(\mathbf{x}')} \times \exp[\mathrm{i}\omega\,p_k(\mathbf{x},\boldsymbol{\gamma})\,(x_k - x'_k)] \quad . \tag{33}$$

The integrand is, except for the aperture weighting factor $a(\mathbf{x}'')$ and the reciprocal transmission coefficient $T(\mathbf{x}'',\mathbf{x})$ between target point $\mathbf{x}$ and receiver point $\mathbf{x}''$, independent of $\mathbf{x}''$.

We denote the angular domain (aperture) corresponding to all rays leading to the receiver area by Γ. The *aperture weighting function*

$$\begin{aligned} &\boldsymbol{\gamma} \in \Gamma: \quad A(\mathbf{x},\boldsymbol{\gamma}) = a(\mathbf{x}'')\;[T(\mathbf{x}'',\mathbf{x})]^2 \\ &\boldsymbol{\gamma} \notin \Gamma: \quad A(\mathbf{x},\boldsymbol{\gamma}) = 0 \end{aligned} \tag{34}$$

accounts both for the aperture limitation to directions $\boldsymbol{\gamma} \in \Gamma$, for possible windowing $a(\mathbf{x}'')$ of the seismic records (time sections) at receiver points $\mathbf{x}''$, and for the two–way accumulated reciprocal transmission coefficient between target point $\mathbf{x}'$ and receiver point $\mathbf{x}''$.

Integration over surface S in Eq. (33) may thus be extended to the whole solid angle (all directions):

$$\widehat{D}_{im}(\mathbf{x},\mathbf{x}',\omega) \approx \frac{\mathrm{i}\omega\widehat{\delta}(\omega)}{8\pi^2}\oint \mathrm{d}\Gamma\,A(\mathbf{x},\boldsymbol{\gamma})\,\frac{e_i(\mathbf{x},\boldsymbol{\gamma})e_m(\mathbf{x}',\boldsymbol{\gamma}')}{[c(\mathbf{x},\boldsymbol{\gamma})]^3\,\varrho(\mathbf{x}')}\,\exp[\mathrm{i}\omega\,p_k(\mathbf{x},\boldsymbol{\gamma})\,(x_k - x'_k)] \quad . \tag{35}$$

The back–propagated scattered wavefield $\widehat{U}_i(\mathbf{x},\omega)$ may be obtained from relation (22) by means of inserting Eq. (35),

$$\widehat{U}_i(\mathbf{x},\omega) \approx \frac{(\mathrm{i}\omega)^3}{8\pi^2}\int \mathrm{d}\mathbf{x}' \oint \mathrm{d}\Gamma\,A(\mathbf{x},\boldsymbol{\gamma})\,\frac{e_i(\mathbf{x},\boldsymbol{\gamma})e_m(\mathbf{x}',\boldsymbol{\gamma}')}{[c(\mathbf{x},\boldsymbol{\gamma})]^3\,\varrho(\mathbf{x}')} \times [\delta c_{mjkl}(\mathbf{x}')p_j(\mathbf{x}',\boldsymbol{\gamma}')\widehat{u}_k(\mathbf{x}',\omega)P_l(\mathbf{x}') - \delta\varrho(\mathbf{x}')\widehat{u}_m(\mathbf{x}',\omega)]\exp[\mathrm{i}\omega\,p_k(\mathbf{x},\boldsymbol{\gamma})\,(x_k - x'_k)] \; . \tag{36}$$

We insert assumption (14) into Eq. (36), and obtain

$$\widehat{U}_i(\mathbf{x},\omega) \approx \frac{(\mathrm{i}\omega)^3}{8\pi^2}\int \mathrm{d}\mathbf{x}' \oint \mathrm{d}\Gamma\,A(\mathbf{x},\boldsymbol{\gamma})\,\frac{e_i(\mathbf{x},\boldsymbol{\gamma})e_m(\mathbf{x}',\boldsymbol{\gamma}')}{[c(\mathbf{x},\boldsymbol{\gamma})]^3\,\varrho(\mathbf{x}')}\,\widehat{f}(\mathbf{x}',\omega) \times [\delta c_{mjkl}(\mathbf{x}')p_j(\mathbf{x}',\boldsymbol{\gamma}')E_k(\mathbf{x}')P_l(\mathbf{x}') - \delta\varrho(\mathbf{x}')E_m(\mathbf{x}')]\,\exp[\mathrm{i}\omega\,p_k(\mathbf{x},\boldsymbol{\gamma})\,(x_k - x'_k)] \quad . \tag{37}$$

We now define the *angle–dependent reflectivity function*

$$r(\mathbf{x}',\boldsymbol{\gamma}') = \frac{\delta\varrho(\mathbf{x}')E_m(\mathbf{x}')e_m(\mathbf{x}',\boldsymbol{\gamma}') - \delta c_{ijkl}(\mathbf{x}')P_i(\mathbf{x}')E_j(\mathbf{x}')p_k(\mathbf{x}',\boldsymbol{\gamma}')e_l(\mathbf{x}',\boldsymbol{\gamma}')}{2\;\varrho(\mathbf{x}')} \quad , \tag{38}$$

and Eq. (37) reads

$$\widehat{U}_i(\mathbf{x},\omega) \approx \frac{-(\mathrm{i}\omega)^3}{4\pi^2}\int\mathrm{d}\mathbf{x}'\oint\mathrm{d}\Gamma\, A(\mathbf{x},\boldsymbol{\gamma})\,\frac{e_i(\mathbf{x},\boldsymbol{\gamma})}{[c(\mathbf{x},\boldsymbol{\gamma})]^3}\,\widehat{f}(\mathbf{x}',\omega)\,r(\mathbf{x}',\boldsymbol{\gamma}')\,\exp[\mathrm{i}\omega\,p_k(\mathbf{x},\boldsymbol{\gamma})\,(x_k-x_k')]\,. \tag{39}$$

The angle–dependent reflectivity function (38) is identical to half the scattering coefficient of *Ursin and Tygel (1997, Eq. 22)* and *Ursin (2004, Eq. 12)*. For the special case of the scattering coefficient in an isotropic medium refer to *Beylkin and Burridge (1990, Fig. 2)* and *Ursin and Tygel (1997, Eq. A.1)*.

Since $\boldsymbol{\gamma}' \approx \boldsymbol{\gamma}$ because points $\mathbf{x}$ and $\mathbf{x}'$ are close, we apply approximation

$$r(\mathbf{x}',\boldsymbol{\gamma}') \approx r(\mathbf{x}',\boldsymbol{\gamma}) \quad . \tag{40}$$

We also apply the first–order paraxial expansion

$$\widehat{f}(\mathbf{x}',\omega) \approx \widehat{f}(\mathbf{x},\omega)\,\exp[\mathrm{i}\omega\,P_k(\mathbf{x})\,(x_k'-x_k)] \tag{41}$$

of the travel time of the incident wave from point $\mathbf{x}$ to point $\mathbf{x}'$. Relation (39) then reads

$$\begin{aligned}\widehat{U}_i(\mathbf{x},\omega) \approx \frac{-(\mathrm{i}\omega)^3}{4\pi^2}\int\mathrm{d}\mathbf{x}'\oint\mathrm{d}\Gamma\, A(\mathbf{x},\boldsymbol{\gamma})\,\frac{e_i(\mathbf{x},\boldsymbol{\gamma})}{[c(\mathbf{x},\boldsymbol{\gamma})]^3}\,\widehat{f}(\mathbf{x},\omega)\\ \times\, r(\mathbf{x}',\boldsymbol{\gamma})\,\exp\big\{\mathrm{i}\omega\,[p_k(\mathbf{x},\boldsymbol{\gamma})-P_k(\mathbf{x})]\,(x_k-x_k')\big\}\quad .\end{aligned} \tag{42}$$

We define the 3–D Fourier transform of the angle–dependent reflectivity function by equation

$$\widehat{r}(\mathbf{k},\boldsymbol{\gamma}) = \widehat{\delta}(\mathbf{k})\int\mathrm{d}\mathbf{x}'\; r(\mathbf{x}',\boldsymbol{\gamma})\;\exp(-\mathrm{i}\,k_k\,x_k') \quad , \tag{43}$$

where constant $\widehat{\delta}(\mathbf{k})$ represents the 3–D Fourier transform of the 3–D Dirac distribution $\delta(\mathbf{x})$. Relation (42) then reads

$$\begin{aligned}\widehat{U}_i(\mathbf{x},\omega) \approx \frac{-(\mathrm{i}\omega)^3\,\widehat{f}(\mathbf{x},\omega)}{4\pi^2\,\widehat{\delta}(\mathbf{k})}\oint\mathrm{d}\Gamma\, A(\mathbf{x},\boldsymbol{\gamma})\frac{e_i(\mathbf{x},\boldsymbol{\gamma})}{[c(\mathbf{x},\boldsymbol{\gamma})]^3}\\ \times\widehat{r}\big(\omega[\mathbf{p}(\mathbf{x},\boldsymbol{\gamma})-\mathbf{P}(\mathbf{x})],\boldsymbol{\gamma}\big)\;\exp\big\{\mathrm{i}\omega\,[p_k(\mathbf{x},\boldsymbol{\gamma})-P_k(\mathbf{x})]\,x_k\big\}\quad .\end{aligned} \tag{44}$$

We transform the back–propagated scattered wavefield into the time domain using inverse 1–D Fourier transform

$$U_i(\mathbf{x},t) = \frac{1}{2\pi\,\widehat{\delta}(\omega)}\int\mathrm{d}\omega\;\widehat{U}_i(\mathbf{x},\omega)\;\exp(-\mathrm{i}\omega t) \quad , \tag{45}$$

and obtain relation

$$\begin{aligned}U_i(\mathbf{x},t) \approx \int\mathrm{d}\omega\;\frac{-(\mathrm{i}\omega)^3\exp(-\mathrm{i}\omega t)\,\widehat{f}(\mathbf{x},\omega)}{8\pi^3\,\widehat{\delta}(\omega)\;\widehat{\delta}(\mathbf{k})}\oint\mathrm{d}\Gamma\, A(\mathbf{x},\boldsymbol{\gamma})\;\frac{e_i(\mathbf{x},\boldsymbol{\gamma})}{[c(\mathbf{x},\boldsymbol{\gamma})]^3}\\ \times\widehat{r}\big(\omega[\mathbf{p}(\mathbf{x},\boldsymbol{\gamma})-\mathbf{P}(\mathbf{x})],\boldsymbol{\gamma}\big)\;\exp\big\{\mathrm{i}\omega\,[p_k(\mathbf{x},\boldsymbol{\gamma})-P_k(\mathbf{x})]\,x_k\big\}\quad .\end{aligned} \tag{46}$$

5. ANALYSIS OF THE MIGRATED SECTION

We assume that imaging functional (8) is linear with respect to the second argument representing the back–propagated scattered wavefield. This is our only assumption about the imaging functional.

5.1. Imaging Function

The polarization of the scattered wavefield back–propagated from the direction given by $\boldsymbol{\gamma}$ is approximately determined by unit vector $e_i(\mathbf{x},\boldsymbol{\gamma})$, see Eq. (46). For the time dependence of the back–propagated scattered wavefield proportional to the local time dependence $f(\mathbf{x},t)$ of incident arrival (14), we define *imaging function*

$$\Phi(\mathbf{x},\boldsymbol{\gamma},\Delta t) = M\big(u_i(\mathbf{x},t'), e_j(\mathbf{x},\boldsymbol{\gamma}) f(\mathbf{x},t+\Delta t)\big) \quad . \tag{47}$$

The imaging function thus expresses the dependence of the migrated section corresponding to the time–shifted normalized back–propagated wavefield $U_j(\mathbf{x},t) = e_j(\mathbf{x},\boldsymbol{\gamma}) f(\mathbf{x},t+\Delta t)$ on time shift Δt.

The Fourier transform of the imaging function reads

$$\widehat{\Phi}(\mathbf{x},\boldsymbol{\gamma},\omega) = \widehat{\delta}(\omega) \int \mathrm{d}\Delta t \; \Phi(\mathbf{x},\boldsymbol{\gamma},\Delta t) \exp(\mathrm{i}\omega\Delta t) \quad . \tag{48}$$

The local time dependence $f(\mathbf{x},t)$ of the incident arrival is related to the local spectrum $\widehat{f}(\mathbf{x},\omega)$ through the inverse Fourier transform

$$f(\mathbf{x},t+\Delta t) = \frac{1}{2\pi\,\widehat{\delta}(\omega')} \int \mathrm{d}\omega' \, \widehat{f}(\mathbf{x},\omega') \exp[-\mathrm{i}\omega'(t+\Delta t)] \quad . \tag{49}$$

We insert Eq. (47) with Eq. (49) into Eq. (48). Since we are assuming that the imaging functional (8) is linear with respect to the second argument, we obtain

$$\widehat{\Phi}(\mathbf{x},\boldsymbol{\gamma},\omega) = \frac{1}{2\pi} \int \mathrm{d}\Delta t \int \mathrm{d}\omega' \, M\big(u_i(\mathbf{x},t'), e_j(\mathbf{x},\boldsymbol{\gamma}) \exp(-\mathrm{i}\omega' t)\big) \, \widehat{f}(\mathbf{x},\omega') \, \exp[\mathrm{i}(\omega-\omega')\Delta t] \, . \tag{50}$$

We integrate over Δt:

$$\widehat{\Phi}(\mathbf{x},\boldsymbol{\gamma},\omega) = \int \mathrm{d}\omega' \, M\big(u_i(\mathbf{x},t'), e_j(\mathbf{x},\boldsymbol{\gamma}) \exp(-\mathrm{i}\omega' t)\big) \, \widehat{f}(\mathbf{x},\omega') \, \delta(\omega'-\omega) \quad . \tag{51}$$

We integrate over ω':

$$\widehat{\Phi}(\mathbf{x},\boldsymbol{\gamma},\omega) = M\big(u_i(\mathbf{x},t'), e_j(\mathbf{x},\boldsymbol{\gamma}) \exp(-\mathrm{i}\omega t)\big) \, \widehat{f}(\mathbf{x},\omega) \quad . \tag{52}$$

5.2. Migrated Section in Terms of the Angle–Dependent Reflectivity Function

We insert the back–propagated scattered wavefield (46) into imaging functional (8), consider Eq. (52), and obtain approximation

$$m^{\mathrm{ArrEW}}(\mathbf{x}) \approx \int \mathrm{d}\omega \, \frac{-(\mathrm{i}\omega)^3}{8\pi^3 \, \widehat{\delta}(\omega) \, \widehat{\delta}(\mathbf{k})} \oint \mathrm{d}\Gamma \, A(\mathbf{x},\boldsymbol{\gamma}) \, \frac{\widehat{\Phi}(\mathbf{x},\boldsymbol{\gamma},\omega)}{[c(\mathbf{x},\boldsymbol{\gamma})]^3} \\ \times \widehat{r}\big(\omega[\mathbf{p}(\mathbf{x},\boldsymbol{\gamma}) - \mathbf{P}(\mathbf{x})],\boldsymbol{\gamma}\big) \exp\big\{\mathrm{i}\omega \, [p_k(\mathbf{x},\boldsymbol{\gamma}) - P_k(\mathbf{x})] \, x_k\big)\big\} \tag{53}$$

of the migrated section. In this approximation, the migrated section is determined by the aperture weighting function (34), by the Fourier transform of imaging function (47), and by the Fourier transform of the angle–dependent reflectivity function (38).

5.3. Migrated Section in Terms of the Reflectivity Function

For each $\mathbf{x}$, vectorial argument $\mathbf{k}$ of the Fourier transform $\widehat{r}(\mathbf{k},\boldsymbol{\gamma})$ of the angle–dependent reflectivity function in relation (53) is parametrized by three parameters $\boldsymbol{\gamma} = (\gamma_1,\gamma_2)$ and ω:

$$\mathbf{k}(\mathbf{x},\boldsymbol{\gamma},\omega) = \omega[\mathbf{p}(\mathbf{x},\boldsymbol{\gamma}) - \mathbf{P}(\mathbf{x})] \quad . \tag{54}$$

We shall refer to wavenumber vector (54) as the *scattering wavenumber vector*. It is often called briefly the "scattering wavenumber" (*Hamran and Lecomte, 1993; Lecomte and Gelius, 1998; Lecomte, 1999*), and sometimes also the "combined wavenumber vector" or the "resolution vector" (*Gelius, 1995a*).

Mapping (54) of $\boldsymbol{\gamma}$ and ω onto $\mathbf{k}$ is not single–valued. On the other hand, mapping (54) is very likely single–valued for $\boldsymbol{\gamma} \in \Gamma$ within angular domains Γ typical for seismic reflection surveys. Especially if the angular difference between direction $\boldsymbol{\gamma}$ corresponding to the ray leading to the source and direction $\boldsymbol{\gamma}$ corresponding to the rays leading to the receivers does not exceed $2\pi/3$ radians. Hereinafter, we shall assume that mapping (54) is single–valued for $\boldsymbol{\gamma} \in \Gamma$.

For each $\mathbf{x}$, arguments $\mathbf{k}$ and $\boldsymbol{\gamma}$ of $\widehat{r}(\mathbf{k},\boldsymbol{\gamma})$ in Eq. (53) are not independent, but are related through Eq. (54). In the vicinity of each point $\mathbf{x}$, we thus define the *local wavenumber–domain reflectivity function* $\widehat{s}(\mathbf{x},\mathbf{k})$ by relation

$$\boxed{\widehat{s}\big(\mathbf{x}, \omega[\mathbf{p}(\mathbf{x},\boldsymbol{\gamma}) - \mathbf{P}(\mathbf{x})]\big) = \widehat{r}\big(\omega[\mathbf{p}(\mathbf{x},\boldsymbol{\gamma}) - \mathbf{P}(\mathbf{x})],\boldsymbol{\gamma}\big)} \tag{55}$$

for scattering wavenumber vectors $\mathbf{k} = \mathbf{k}(\mathbf{x},\boldsymbol{\gamma},\omega)$ parametrized by $\boldsymbol{\gamma}$ and ω. The local wavenumber–domain reflectivity function $\widehat{s}(\mathbf{x},\mathbf{k})$ is defined by Eq. (55) for all $\mathbf{k} = \mathbf{k}(\mathbf{x},\boldsymbol{\gamma},\omega)$ corresponding to $\boldsymbol{\gamma} \in \Gamma$. For other wavenumber vectors $\mathbf{k}$, it may be either defined by Eq. (55) or put equal to zero.

In definition (55), the strong dependence of $\widehat{r}(\mathbf{k},\boldsymbol{\gamma})$ on wavenumber vector $\mathbf{k}$ is essential. On the other hand, even if the dependence of $r(\mathbf{x}',\boldsymbol{\gamma})$ on $\mathbf{x}'$ has the form of the Dirac distribution $\delta(\mathbf{x}')$, the dependence of $r(\mathbf{x}',\boldsymbol{\gamma})$ on $\boldsymbol{\gamma}$ makes the dependence of local reflectivity function $s(\mathbf{x},\mathbf{x}')$ on $\mathbf{x}'$ different from the Dirac distribution $\delta(\mathbf{x}')$.

Note that definition (55) may also be approximated by expression

$$\begin{aligned}\widehat{s}\big(\mathbf{x},\omega[\mathbf{p}(\mathbf{x},\boldsymbol{\gamma})-\mathbf{P}(\mathbf{x})]\big) \approx{}& \widehat{\tfrac{\delta\varrho}{2\,\varrho}}\big(\omega[\mathbf{p}(\mathbf{x},\boldsymbol{\gamma})-\mathbf{P}(\mathbf{x})]\big)E_m(\mathbf{x})e_m(\mathbf{x},\boldsymbol{\gamma})\\ &-\widehat{\tfrac{\delta c_{ijkl}}{2\,\varrho}}\big(\omega[\mathbf{p}(\mathbf{x},\boldsymbol{\gamma})-\mathbf{P}(\mathbf{x})]\big)P_i(\mathbf{x})E_j(\mathbf{x})p_k(\mathbf{x},\boldsymbol{\gamma})e_l(\mathbf{x},\boldsymbol{\gamma})\quad .\end{aligned} \tag{56}$$

This expression results from approximating $P_i(\mathbf{x}')$, $E_j(\mathbf{x}')$, $p_k(\mathbf{x}',\boldsymbol{\gamma}')$, $e_l(\mathbf{x}',\boldsymbol{\gamma}')$ in definition (38) by $P_i(\mathbf{x})$, $E_j(\mathbf{x})$, $p_k(\mathbf{x},\boldsymbol{\gamma}')$, $e_l(\mathbf{x},\boldsymbol{\gamma}')$ and inserting the approximation into definition (55).

We are now going to switch, in approximation (53) of the migrated section, from integration over $\boldsymbol{\gamma}$ and ω to integration over wavenumbers $\mathbf{k}$. The Jacobian of transformation (54) from $\boldsymbol{\gamma}$ and ω to $\mathbf{k}(\mathbf{x},\boldsymbol{\gamma},\omega)$ is

$$\frac{\mathrm{d}\mathbf{k}}{\mathrm{d}\Gamma\mathrm{d}\omega}=\frac{\omega^2}{[c(\mathbf{x},\boldsymbol{\gamma})]^3}|v_i(\mathbf{x},\boldsymbol{\gamma})[p_i(\mathbf{x},\boldsymbol{\gamma})-P_i(\mathbf{x})]|\quad . \tag{57}$$

Note that, for fixed position $\mathbf{x}$, the receivers may be parametrized by angles $\boldsymbol{\gamma}$. For this parametrization, quantity (57) represents the Beylkin determinant (*Beylkin, 1985, Eq. 4.5; Bleistein, 1987, Eq. 5*).

In approximation (53) of the migrated section, the local wavenumber–domain reflectivity function (55) is filtered with the *local wavenumber resolution filter* defined by relation

$$\widehat{w}\big(\mathbf{x},\omega[\mathbf{p}(\mathbf{x},\boldsymbol{\gamma})-\mathbf{P}(\mathbf{x})]\big)=-\frac{A(\mathbf{x},\boldsymbol{\gamma})}{|v_i(\mathbf{x},\boldsymbol{\gamma})[p_i(\mathbf{x},\boldsymbol{\gamma})-P_i(\mathbf{x})]|}\frac{\widehat{\dot{\Phi}}(\mathbf{x},\boldsymbol{\gamma},\omega)}{\widehat{\delta}(\omega)}\,\widehat{\delta}(\mathbf{k}) \tag{58}$$

for all scattering wavenumber vectors $\mathbf{k}=\omega[\mathbf{p}(\mathbf{x},\boldsymbol{\gamma})-\mathbf{P}(\mathbf{x})]$ corresponding to $\boldsymbol{\gamma}\in\Gamma$, and equal to zero for other wavenumber vectors $\mathbf{k}$.

The local wavenumber resolution filter (58) is specified in terms of the aperture weighting function (34) and 1–D Fourier transform

$$\widehat{\dot{\Phi}}(\mathbf{x},\boldsymbol{\gamma},\omega)=-\mathrm{i}\omega\,\widehat{\Phi}(\mathbf{x},\boldsymbol{\gamma},\omega) \tag{59}$$

of the derivative $\dot{\Phi}(\mathbf{x},\boldsymbol{\gamma},\Delta t)$ of the imaging function.

In definition (58), the dependence of $\widehat{w}(\mathbf{x},\mathbf{k})$ along lines $\mathbf{k}=\omega[\mathbf{p}(\mathbf{x},\boldsymbol{\gamma})-\mathbf{P}(\mathbf{x})]$ parametrized by ω is determined just by the dependence of $\widehat{\dot{\Phi}}(\mathbf{x},\boldsymbol{\gamma},\omega)$ on ω. This dependence together with the aperture specified by the dependence of the aperture weighting function $A(\mathbf{x},\boldsymbol{\gamma})$ on $\boldsymbol{\gamma}$ determine the essential properties of the local wavenumber resolution filter (58), which was already observed by *Devaney and Oristaglio (1984)*, *Wu and Toksöz (1987)* or *Dickens and Winbow (1991)*.

The dependence of $\widehat{\dot{\Phi}}$, p_k and v_l on $\boldsymbol{\gamma}$ is moderate. For a sufficiently narrow aperture, $\widehat{\dot{\Phi}}$, p_k and v_l on the right–hand side of definition (58) may even be approximated by their mean values with respect to $\boldsymbol{\gamma}$.

The dependence of A, $\widehat{\dot{\Phi}}$, P_k, p_k and v_l on $\mathbf{x}$ is also moderate. For a sufficiently small target zone, A, $\widehat{\dot{\Phi}}$, P_k, p_k and v_l on the right–hand side of definition (58) may even be approximated by their mean values with respect to $\mathbf{x}$, and the local wavenumber resolution filter $\widehat{w}(\mathbf{x},\mathbf{k})\approx\widehat{w}(\overline{\mathbf{x}},\mathbf{k})$ becomes independent of position $\mathbf{x}$.

Approximation (53) of the migrated section then reads

$$m^{\mathrm{ArrEW}}(\mathbf{x}) \approx \int \mathrm{d}\omega \, \frac{\omega^2}{8\pi^3 \, \widehat{\delta}(\mathbf{k})} \oint \mathrm{d}\Gamma \, \frac{|v_i(\mathbf{x},\boldsymbol{\gamma})[p_i(\mathbf{x},\boldsymbol{\gamma}) - P_i(\mathbf{x})]|}{[c(\mathbf{x},\boldsymbol{\gamma})]^3 \, \widehat{\delta}(\mathbf{k})} \, \widehat{w}\big(\mathbf{x}, \omega[\mathbf{p}(\mathbf{x},\boldsymbol{\gamma}) - \mathbf{P}(\mathbf{x})]\big)$$
$$\times \widehat{s}\big(\mathbf{x}, \omega[\mathbf{p}(\mathbf{x},\boldsymbol{\gamma}) - \mathbf{P}(\mathbf{x})]\big) \exp\{\mathrm{i}\omega \, [p_k(\mathbf{x},\boldsymbol{\gamma}) - P_k(\mathbf{x})] \, x_k)\} \quad . \tag{60}$$

We insert substitutions (54) and (57) into approximation (60). The migrated section then has the form of integral operator

$$m^{\mathrm{ArrEW}}(\mathbf{x}) \approx \frac{1}{8\pi^3 \, \widehat{\delta}(\mathbf{k})} \int \mathrm{d}\mathbf{k} \, \frac{\widehat{w}(\mathbf{x},\mathbf{k}) \, \widehat{s}(\mathbf{x},\mathbf{k})}{\widehat{\delta}(\mathbf{k})} \, \exp(\mathrm{i} \, k_k \, x_k) \quad . \tag{61}$$

The right–hand side of relation (61) locally has the character of the Fourier transform of convolution.

We define the inverse Fourier transform of wavenumber–domain function $\widehat{s}(\mathbf{x},\mathbf{k})$ by relation

$$s(\mathbf{x},\mathbf{x}') \frac{1}{8\pi^3 \, \widehat{\delta}(\mathbf{k})} \int \mathrm{d}\mathbf{k} \, \widehat{s}(\mathbf{x},\mathbf{k}) \, \exp(\mathrm{i} \, k_k \, x'_k) \quad . \tag{62}$$

We analogously define the *local resolution function* $w(\mathbf{x},\mathbf{x}')$ as the inverse Fourier transform of the local wavenumber resolution filter $\widehat{w}(\mathbf{x},\mathbf{k})$ given by Eq. (58), and express approximation (61) in the spatial domain:

$$m^{\mathrm{ArrEW}}(\mathbf{x}) \approx \int \mathrm{d}\mathbf{x}' \, w(\mathbf{x}, \mathbf{x}-\mathbf{x}') \, s(\mathbf{x},\mathbf{x}') \quad . \tag{63}$$

The right–hand side of relation (63) locally has the character of convolution. Since the dependence of function $s(\mathbf{x},\mathbf{x}')$ on $\mathbf{x}$ is moderate, we may use approximation

$$s(\mathbf{x},\mathbf{x}') \approx s(\mathbf{x}',\mathbf{x}') \tag{64}$$

for all points $\mathbf{x}$ from the vicinity of point $\mathbf{x}'$. The dependence of $s(\mathbf{x},\mathbf{x}')$ on $\mathbf{x}$ becomes evident on a global rather than local scale. For each $\mathbf{x}$, the local resolution function $w(\mathbf{x},\mathbf{x}-\mathbf{x}')$ is concentrated in the vicinity of point $\mathbf{x}' = \mathbf{x}$. Because of this localization, we may insert approximation (64) into relation (63), and obtain expression

$$\boxed{m^{\mathrm{ArrEW}}(\mathbf{x}) \approx \int \mathrm{d}\mathbf{x}' \, w(\mathbf{x}, \mathbf{x}-\mathbf{x}') \, r(\mathbf{x}')} \tag{65}$$

for the migrated section. Here

$$\boxed{r(\mathbf{x}') = s(\mathbf{x}',\mathbf{x}')} \tag{66}$$

is the *reflectivity function*. This reflectivity function is angle–independent for a common shot, but changes with the source position.

In approximation (65), the dependence of the local resolution function $w(\mathbf{x}, \mathbf{x}–\mathbf{x}')$ on coordinate difference $\mathbf{x}-\mathbf{x}'$ is essential, whereas its dependence on position $\mathbf{x}$ is moderate and becomes evident on a global rather than local scale.

If the reflectivity function $r(\mathbf{x}')$ had the form of the Dirac distribution $\delta(\mathbf{x}'-\mathbf{x}^0)$, the migrated section would read $m^{\mathrm{ArrEW}}(\mathbf{x}) \approx w(\mathbf{x}, \mathbf{x}-\mathbf{x}^0)$. That is why the local resolution function $w(\mathbf{x}, \mathbf{x}')$ is often referred to as the point–spread function (*Devaney, 1984; Gelius et al., 1991; Gelius, 1995a; 1995b*).

For the figures of the local resolution functions in acoustic media refer to *Devaney (1984)*, *Wu and Toksöz (1987)*, *Pratt and Worthington (1988)*, *Hamran and Lecomte (1993)*, *Lecomte and Gelius (1998)* and *Lecomte (1999)*.

Since convolution (65) images the gradient of reflectivity function $r(\mathbf{x}')$ rather than the reflectivity function itself, we shall express the migrated section also in terms of the spatial distribution of the weak–contrast displacement reflection–transmission coefficient.

5.4. Migrated Section in Terms of the Reflection–Transmission Coefficient

We define locally, for points $\mathbf{x}'$ from the vicinity of point $\mathbf{x}$, the angle–dependent distribution

$$R(\mathbf{x}, \mathbf{x}', \boldsymbol{\gamma}) = \frac{r_{,k}(\mathbf{x}', \boldsymbol{\gamma})}{|v_i(\mathbf{x}, \boldsymbol{\gamma})\,[p_i(\mathbf{x}, \boldsymbol{\gamma}) - P_i(\mathbf{x})]|} \, \frac{[p_k(\mathbf{x}, \boldsymbol{\gamma}) - P_k(\mathbf{x})]}{|\mathbf{p}(\mathbf{x}, \boldsymbol{\gamma}) - \mathbf{P}(\mathbf{x})|} \tag{67}$$

of the weak–contrast displacement reflection–transmission coefficient. Partial derivatives $r_{,k}$ in definition (67) are related to variable $\mathbf{x}'$.

The Fourier transform of function (67), analogous to Fourier transform (43), reads

$$\widehat{R}(\mathbf{x}, \mathbf{k}, \boldsymbol{\gamma}) = \frac{\widehat{r}(\mathbf{k}, \boldsymbol{\gamma})}{|v_i(\mathbf{x}, \boldsymbol{\gamma})\,[p_i(\mathbf{x}, \boldsymbol{\gamma}) - P_i(\mathbf{x})]|} \, \mathrm{i}k_k \, \frac{[p_k(\mathbf{x}, \boldsymbol{\gamma}) - P_k(\mathbf{x})]}{|\mathbf{p}(\mathbf{x}, \boldsymbol{\gamma}) - \mathbf{P}(\mathbf{x})|} \quad . \tag{68}$$

Analogously to definition (55), we define for each point $\mathbf{x}$ the *local wavenumber distribution of the weak–contrast displacement reflection–transmission coefficient* by relation

$$\widehat{S}\big(\mathbf{x}, \omega[\mathbf{p}(\mathbf{x}, \boldsymbol{\gamma}) - \mathbf{P}(\mathbf{x})]\big) = \widehat{R}\big(\mathbf{x}, \omega[\mathbf{p}(\mathbf{x}, \boldsymbol{\gamma}) - \mathbf{P}(\mathbf{x})], \boldsymbol{\gamma}\big) \quad . \tag{69}$$

We insert Eq. (68) into Eq. (69) and obtain relation

$$\widehat{S}\big(\mathbf{x}, \omega[\mathbf{p}(\mathbf{x}, \boldsymbol{\gamma}) - \mathbf{P}(\mathbf{x})]\big) = \widehat{r}\big(\omega[\mathbf{p}(\mathbf{x}, \boldsymbol{\gamma}) - \mathbf{P}(\mathbf{x})], \boldsymbol{\gamma}\big) \, \frac{\mathrm{i}\omega \, |\mathbf{p}(\mathbf{x}, \boldsymbol{\gamma}) - \mathbf{P}(\mathbf{x})|}{|v_i(\mathbf{x}, \boldsymbol{\gamma})\,[p_i(\mathbf{x}, \boldsymbol{\gamma}) - P_i(\mathbf{x})]|} \quad . \tag{70}$$

The *local wavenumber resolution filter* analogous to filter (58), but corresponding to the local wavenumber distribution (70) of the weak–contrast displacement reflection–transmission coefficient, is defined by relation

$$\widehat{W}\big(\mathbf{x}, \omega[\mathbf{p}(\mathbf{x}, \boldsymbol{\gamma}) - \mathbf{P}(\mathbf{x})]\big) = \frac{A(\mathbf{x}, \boldsymbol{\gamma})}{|\mathbf{p}(\mathbf{x}, \boldsymbol{\gamma}) - \mathbf{P}(\mathbf{x})|} \, \frac{\widehat{\Phi}(\mathbf{x}, \boldsymbol{\gamma}, \omega)}{\widehat{\delta}(\omega)} \, \widehat{\delta}(\mathbf{k}) \tag{71}$$

for scattering wavenumber vectors $\mathbf{k} = \omega[\mathbf{p}(\mathbf{x}, \boldsymbol{\gamma}) - \mathbf{P}(\mathbf{x})]$ corresponding to $\boldsymbol{\gamma} \in \Gamma$, and is equal to zero for other wavenumber vectors $\mathbf{k}$.

If we compare local wavenumber resolution filters (58) and (71), we see that filter (71) is specified in terms of imaging function $\Phi(\mathbf{x},\boldsymbol{\gamma},\Delta t)$ rather than in terms of its derivative (59). Note that denominator $|\mathbf{p}(\mathbf{x},\boldsymbol{\gamma})-\mathbf{P}(\mathbf{x})|$ in Eq. (71) is called the stretch factor (*Ursin, 2004*) and characterizes stretching determined by Eq. (54).

Analogously to relation (61), we approximate the migrated section by integral operator

$$m^{\mathrm{ArrEW}}(\mathbf{x}) \approx \frac{1}{8\pi^3\,\widehat{\delta}(\mathbf{k})}\int \mathrm{d}\mathbf{k}\;\frac{\widehat{W}(\mathbf{x},\mathbf{k})\;\widehat{S}(\mathbf{x},\mathbf{k})}{\widehat{\delta}(\mathbf{k})}\;\exp(\mathrm{i}\,k_k\,x_k)\quad . \tag{72}$$

The right–hand side of relation (72) has locally the character of the Fourier transform of convolution.

We define the inverse Fourier transform of wavenumber–domain functions $\widehat{W}(\mathbf{x},\mathbf{k})$ and $\widehat{S}(\mathbf{x},\mathbf{k})$ by relations analogous to relation (62), and express approximation (72) in the spatial domain:

$$m^{\mathrm{ArrEW}}(\mathbf{x}) \approx \int \mathrm{d}\mathbf{x}'\;W(\mathbf{x},\mathbf{x}-\mathbf{x}')\;S(\mathbf{x},\mathbf{x}')\quad . \tag{73}$$

The right–hand side of relation (73) has again locally the character of convolution. Since the dependence of function $S(\mathbf{x},\mathbf{x}')$ on $\mathbf{x}$ is moderate, we may use approximation

$$S(\mathbf{x},\mathbf{x}') \approx S(\mathbf{x}',\mathbf{x}') \tag{74}$$

for all points $\mathbf{x}$ from the vicinity of point $\mathbf{x}'$. The dependence of $S(\mathbf{x},\mathbf{x}')$ on $\mathbf{x}$ becomes evident on a global rather than local scale. For each $\mathbf{x}$, the local resolution function $W(\mathbf{x},\mathbf{x}-\mathbf{x}')$ is concentrated in the vicinity of point $\mathbf{x}'=\mathbf{x}$. Because of this localization, we may insert approximation (74) into relation (73), and obtain expression

$$\boxed{m^{\mathrm{ArrEW}}(\mathbf{x}) \approx \int \mathrm{d}\mathbf{x}'\;W(\mathbf{x},\mathbf{x}-\mathbf{x}')\;R(\mathbf{x}')} \tag{75}$$

for the migrated section. Here

$$\boxed{R(\mathbf{x}') = S(\mathbf{x}',\mathbf{x}')} \tag{76}$$

is the *spatial distribution of the weak–contrast displacement reflection–transmission coefficient*.

For example, in a case of a single planar interface $x_3 = x_3^0$ between two homogeneous media, the singular function of the reflecting surface (*Ursin, 2004, Eq. 41*) reads $\delta(x_3-x_3^0)$, and the spatial distribution of the weak–contrast displacement reflection–transmission coefficient is $R(\mathbf{x}) = R(x_1,x_2)\;\delta(x_3-x_3^0)$, where $R(x_1,x_2)$ is the weak–contrast displacement reflection–transmission coefficient of *Klimeš (2003, Eq. 71)* corresponding to the direction of the incident wavefield at (x_1,x_2,x_3^0). Within the Born approximation used throughout this paper, the weak–contrast displacement reflection–transmission coefficient $R(x_1,x_2)$ is, naturally, the approximation of the plane–wave displacement reflection–transmission coefficient (*Červený*

and Ravindra, 1971) for very small contrasts of material parameters. For P–P scattering in isotropic media, the weak–contrast displacement reflection–transmission coefficient $R(x_1, x_2)$ is equivalent to the reflection coefficient of *Stolt and Benson (1986, Eq. 1.7)*.

Approximation (75) has locally the character of convolution, because the dependence of the local resolution function $W(\mathbf{x}, \mathbf{x}-\mathbf{x}')$ on the coordinate difference $\mathbf{x}-\mathbf{x}'$ is essential, whereas the dependence of $W(\mathbf{x}, \mathbf{x}-\mathbf{x}')$ on position $\mathbf{x}$ is moderate and becomes evident on a global rather than local scale.

5.5. Isotropic Elastic Media

In isotropic elastic media, where

$$c_{ijkl}(\mathbf{x}') = \lambda(\mathbf{x}')\,\delta_{ij}\delta_{kl} + \mu(\mathbf{x}')\,[\delta_{ik}\delta_{jl} + \delta_{il}\delta_{jk}] \quad , \tag{77}$$

the angle–dependent reflectivity function (38) reads

$$\begin{aligned} r(\mathbf{x}',\boldsymbol{\gamma}') = \big\{ & \delta\varrho(\mathbf{x}')E_m(\mathbf{x}')e_m(\mathbf{x}',\boldsymbol{\gamma}') - \delta\lambda(\mathbf{x}')\,P_i(\mathbf{x}')E_i(\mathbf{x}')p_j(\mathbf{x}',\boldsymbol{\gamma}')e_j(\mathbf{x}',\boldsymbol{\gamma}') \\ & - \delta\mu(\mathbf{x}')\,[P_i(\mathbf{x}')p_i(\mathbf{x}',\boldsymbol{\gamma}')E_j(\mathbf{x}')e_j(\mathbf{x}',\boldsymbol{\gamma}') + P_i(\mathbf{x}')e_i(\mathbf{x}',\boldsymbol{\gamma}')E_j(\mathbf{x}')p_j(\mathbf{x}',\boldsymbol{\gamma}')]\big\} \\ & / \,[2\,\varrho(\mathbf{x}')] \quad . \end{aligned} \tag{78}$$

In acoustic media with constant density, where $\delta\mu(\mathbf{x}') = 0$, $\delta\lambda(\mathbf{x}') = \varrho(\mathbf{x}')\,\delta[v^2(\mathbf{x}')]$, $\delta\varrho(\mathbf{x}') = 0$, $P_i(\mathbf{x}') = E_i(\mathbf{x}')/v(\mathbf{x}')$ and $p_i(\mathbf{x}') = e_i(\mathbf{x}')/v(\mathbf{x}')$, reflectivity function (78) becomes angle–independent:

$$r(\mathbf{x}',\boldsymbol{\gamma}') = -\frac{\delta[v^2(\mathbf{x}')]}{2\,v^2(\mathbf{x}')} \quad . \tag{79}$$

6. NUMERICAL EXAMPLES

The effect of convolution (65) on the structure in Fig. 1 is demonstrated in Figs. 4 and 5 for the scalar wave equation in 2–D acoustic media with constant density. Fig. 1 displays small velocity perturbations to a homogeneous velocity model. Figs. 2 and 3 show considered measurement configurations. Figs. 4–6 then show the images of the velocity which can ideally be obtained by prestack depth migration for a given configuration and source time function, see the corresponding figure captions for details.

7. CONCLUSIONS

We have studied the physical meaning of the migrated sections, independently of a particular migration algorithm. The derived expressions demonstrate that the 3–D common–shot elastic prestack depth migrated section can approximately be represented by the convolution (65) of the reflectivity function (66) with the corresponding local resolution function determined by expression (58). Equivalently, the migrated section can also be approximately represented by the convolution

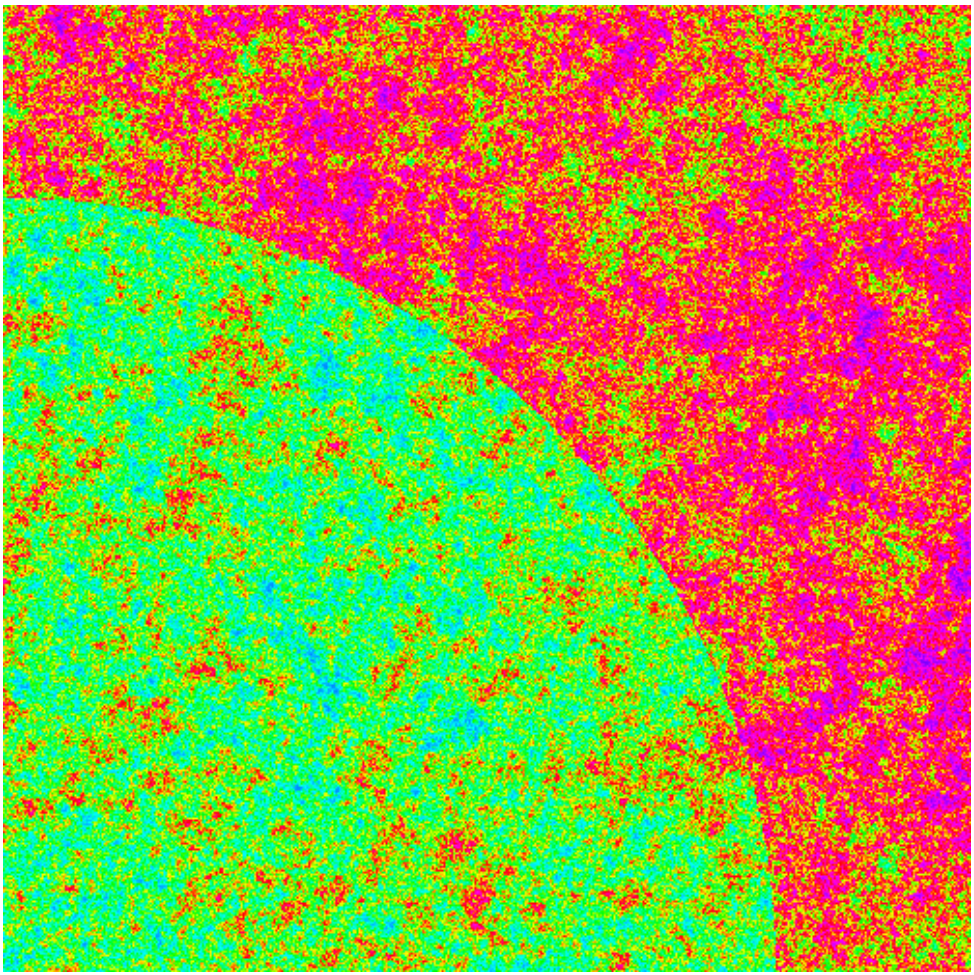

Fig. 1. Structure of the target zone. A homogeneous quarter circle is superposed on a randomly generated representation of the self–affine medium in order to supplement random heterogeneities with a sharp interface. The target zone is assumed small compared with its depth below the source and receivers.

(75) of the spatial distribution (76) of the weak–contrast displacement reflection–transmission coefficient with the corresponding local resolution function determined by expression (71).

Both the reflectivity function (66) and the spatial distribution (76) of the weak–contrast displacement reflection–transmission coefficient are defined in terms of the angle–dependent reflectivity function (38), whose angular dependence has been transformed to the spatial dependence using Eqs. (55) and (69). Both these functions (66) and (76) approximately specify the linear combination of the perturbations of elastic moduli and density to which the migrated section is *sensitive*.

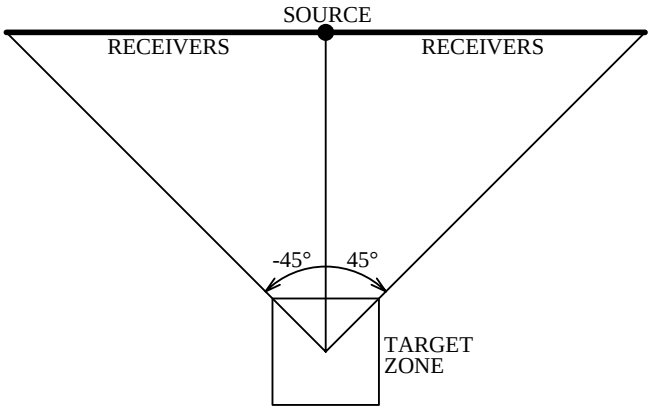

Fig. 2. The first source–receiver configuration. The length of the symmetric receiver profile, with the source above the target zone (angle 0°), is twice the depth of the target zone, which corresponds to the aperture from -45° to 45°.

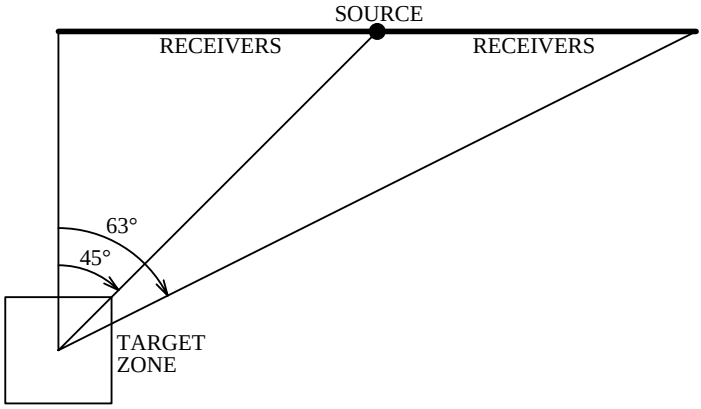

Fig. 3. The second source–receiver configuration. The symmetric receiver profile from Fig. 2 has been shifted to the right, locating the leftmost receiver above the target zone. The source is thus in the direction of 45° and the aperture extends from 0° to 63°.

The *resolution* of the linear combination of the perturbations of elastic moduli and density in the migrated section is determined by the corresponding local resolution function. The local resolution functions are considerably sensitive to heterogeneity. The local resolution functions in elastic media fundamentally differ from their acoustic counterparts, especially by the existence of converted scattered waves in elastic media. On the other hand, the local resolution functions are not influenced too much by anisotropy if the anisotropy is correctly included in the velocity model and the migration algorithm, see Eqs. (58) and (71).

Using these results, we can predict *approximately* the migration resolution without doing the whole and expensive migration. The explicit approximate expressions for the reflectivity function (66) and for the spatial distribution (76) of the weak–

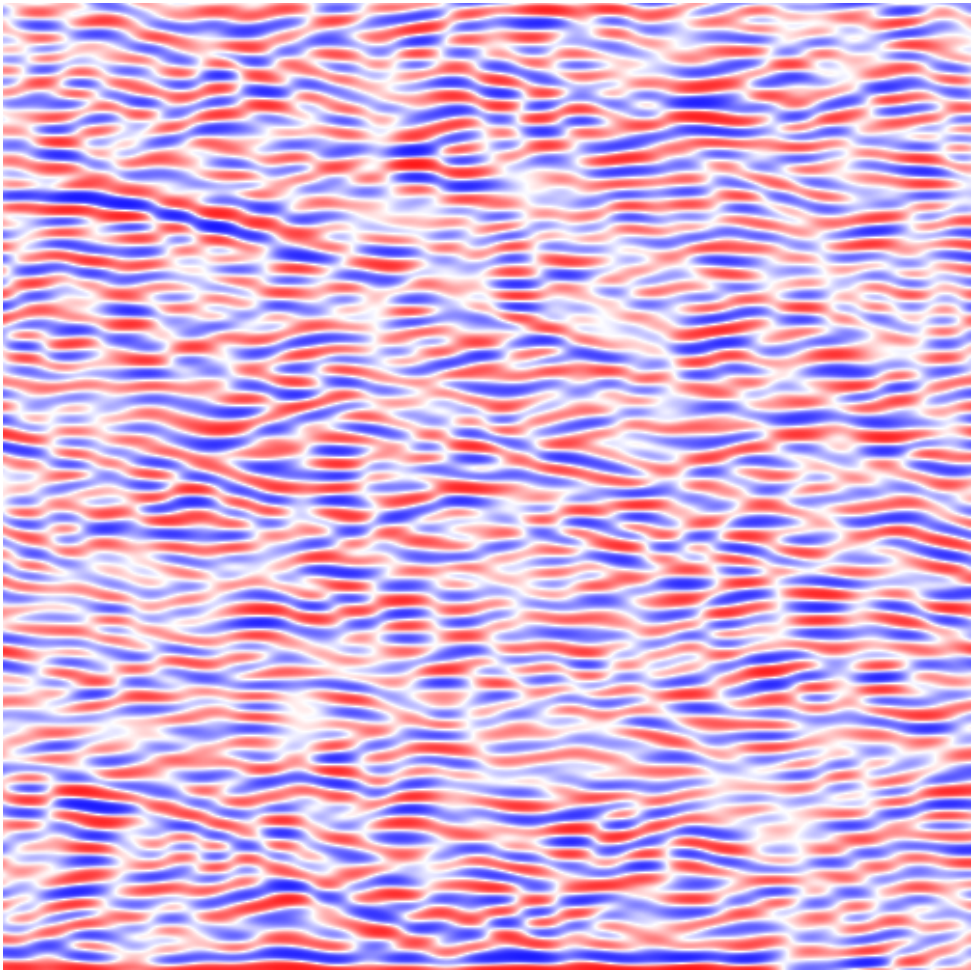

Fig. 4. Common–shot prestack depth migrated section of the structure displayed in Fig. 1, simulated according to Eq. (65) in a homogeneous velocity model for the first source–receiver configuration displayed in Fig. 2. The imaging function is the Gabor signal with the predominant wavelength of 6% of the target zone dimension. The length of the symmetric receiver profile, with the source above the target zone (angle 0°), is twice the depth of the target zone, which corresponds to the aperture from -45° to 45°. Only wavenumber vectors between -22.5° and 22.5° are thus present in the image.

contrast displacement reflection–transmission coefficient enable us to approximately determine which linear combination of the perturbations of elastic moduli and density is imaged for the given measurement configuration, see Eqs. (38), (55), and (69) with (67). The explicit approximate wavenumber–domain expressions (58) and (71) for the corresponding local resolution functions enable us to understand how the migration resolution depends on the measurement configuration.

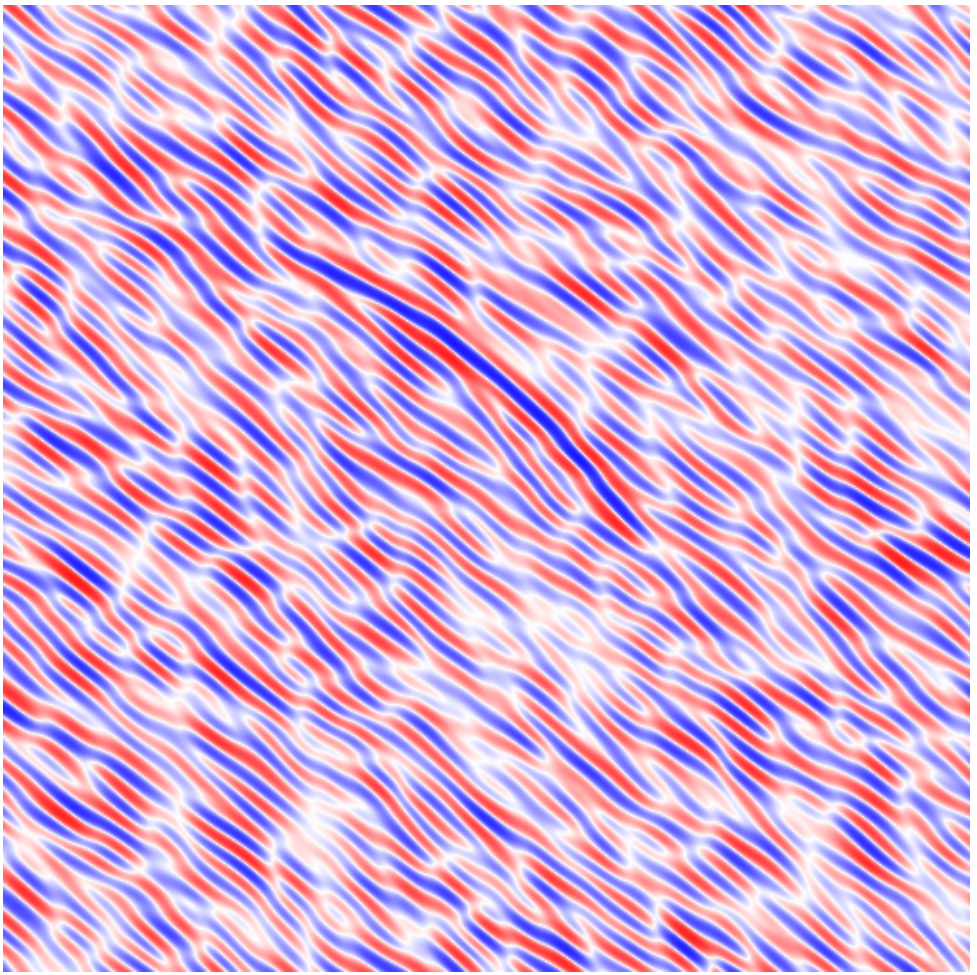

Fig. 5. Common–shot prestack depth migrated section of the structure displayed in Fig. 1, simulated according to Eq. (65) in a homogeneous velocity model for the second source–receiver configuration displayed in Fig. 3. The symmetric receiver profile has been shifted to the right, locating the leftmost receiver above the target zone. The source is thus in the direction of 45° and the aperture extends from 0° to 63°. Only wavenumber vectors between 22.5° and 54° are thus present in the image.

Acknowledgements: This paper is dedicated to Vlastislav Červený who introduced me to elastic wave propagation and the ray theory in particular. My theoretical research has been enabled by his long–term wise and patient guidance.

I am indebted to Paul Spudich who provided me with his perfect code I could modify to calculate the numerical examples presented here. I am grateful to two anonymous reviewers and associate editor Petr Jílek whose suggestions made it possible for me to improve the

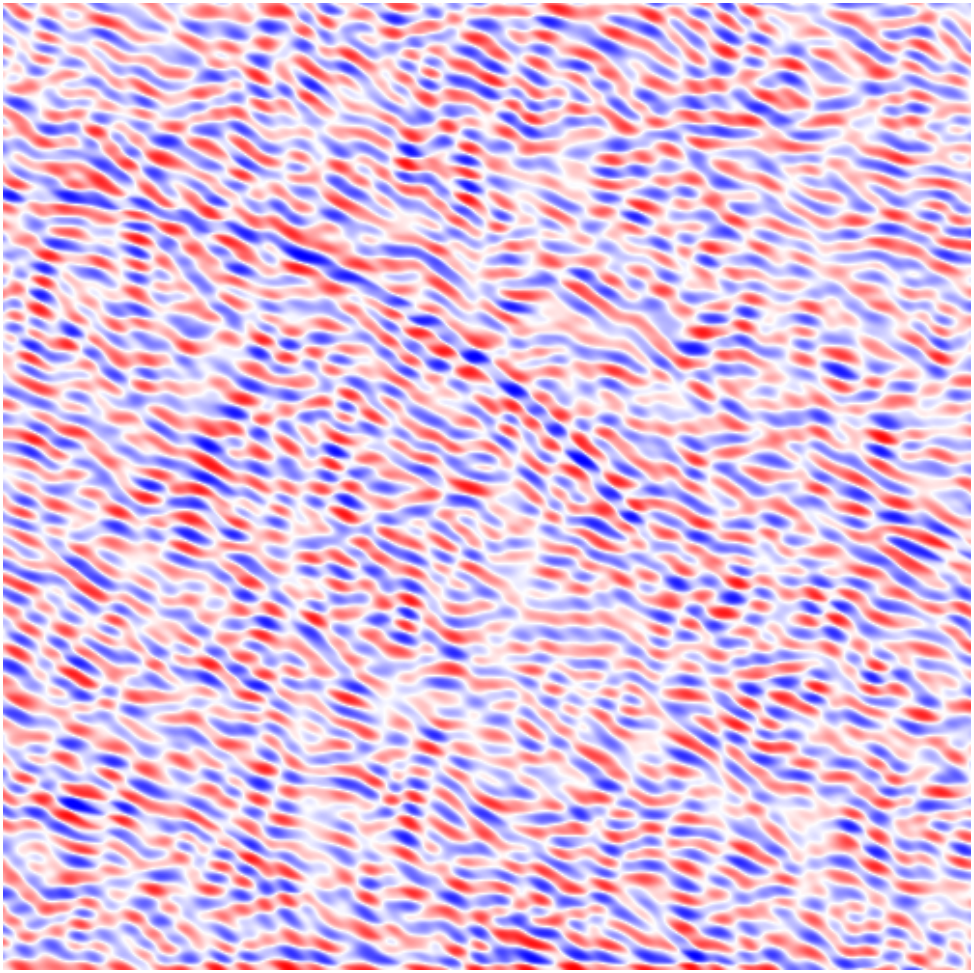

Fig. 6. Sum of the common–shot prestack depth migrated sections of Figs. 4 and 5. Let us emphasize that Figs. 4–6 are not the result of a particular migration: they show which features of the structure can be resolved by the ideal migration (no multiples, no noise, no transmission losses, perfect velocity model, exact calculation of elastic wavefields).

paper. I also thank editor–in–chief Ivan Pšenčík and technical editor Eduard Petrovský for their assistance in preparing the final version of the paper.

The research has been supported by the Grant Agency of the Czech Republic under contracts 205/95/1465 and P210/10/0736, by the Ministry of Education of the Czech Republic within research project MSM0021620860, and by the members of the consortium "Seismic Waves in Complex 3–D Structures" (see "http://sw3d.cz").

References

Beylkin G., 1985. Imaging of discontinuities in the inverse scattering problem by inversion of a causal generalized Radon transform. *J. Math. Phys.*, **26**, 99–108.

Beylkin G. and Burridge R, 1990. Linearized inverse scattering problems in acoustics and elasticity. *Wave Motion*, **12**, 15–52.

Bleistein N., 1987. On the imaging of reflectors in the earth. *Geophysics*, **52**, 931–942.

Červený V., 2001. *Seismic Ray Theory.* Cambridge University Press, Cambridge, U.K.

Červený V. and Ravindra R., 1971. *Theory of Seismic Head Waves.* University Toronto Press, Toronto.

Claerbout J.F., 1971. Toward a unified theory of reflector mapping. *Geophysics*, **36**, 467–481.

Devaney A.J., 1984. Geophysical diffraction tomography. *IEEE Trans. Geosci. Remote Sens.*, **22**, 3–13.

Devaney A.J. and Oristaglio M.L., 1984. Geophysical diffraction tomography. *SEG Expanded Abstracts*, **3**, 330-333 (*Expanded Abstracts of 54th Annual Meeting, Atlanta*, Soc. Explor. Geophysicists, Tulsa).

Dickens T.A. and Winbow, G.A., 1991. Study of geophysical diffraction tomography. *SEG Expanded Abstracts*, **10**, 963-966 (*Expanded Abstracts of 61nd Annual Meeting, Houston*, Soc. Explor. Geophysicists, Tulsa).

Gelius L.-J., 1995a. Generalized acoustic diffraction tomography. *Geophys. Prospect.*, **43**, 3–29.

Gelius L.-J., 1995b. Limited–view diffraction tomography in a nonuniform background. *Geophysics*, **60**, 580–588.

Gelius L.-J., Johansen I., Sponheim N. and Stamnes J.J., 1991. A generalized diffraction tomography algorithm. *J. Acoust. Soc. Amer.*, **89**, 523–528.

Hamran S-E. and Lecomte I., 1993. Local plane–wavenumber diffraction tomography in heterogeneous backgrounds. *J. Seism. Explor.*, **2**, 133-146.

Klimeš L., 2003. Weak–contrast reflection–transmission coefficients in a generally anisotropic background. *Geophysics*, **68**, 2063–2072 (online at http://sw3d.cz).

Lecomte I., 1999. Local and controlled prestack depth migration in complex areas. *Geophys. Prospect.*, **47**, 799–818.

Lecomte I. and Gelius L.-J., 1998. Have a look at the resolution of prestack depth migration for any model, survey and wavefield. *SEG Expanded Abstracts*, **17**, 1112-1115 (*Expanded Abstracts of 68th Annual Meeting, New Orleans*, Soc. Explor. Geophysicists, Tulsa).

Pratt R.G. and Worthington M.H., 1988. The application of diffraction tomography to cross–hole seismic data. *Geophysics*, **53**, 1284–1294.

Schleicher J., Tygel M., Ursin B. and Bleistein N., 2001. The Kirchhoff–Helmholtz integral for anisotropic elastic media. *Wave Motion*, **34**, 353–364.

Stolt R.H. and Benson A.K., 1986. *Seismic Migration. Theory and Practice.* Geophysical Press, London–Amsterdam.

Ursin B., 2004. Tutorial: Parameter inversion and angle migration in anisotropic elastic media. *Geophysics*, **69**, 1125–1142.

Ursin B. and Tygel M., 1997. Reciprocal volume and surface scattering integrals for anisotropic elastic media. *Wave Motion*, **26**, 31–42.

Wu R.-S. and Toksöz M.N., 1987. Diffraction tomography and multisource holography applied to seismic imaging. *Geophysics*, **52**, 11–25.